energies

MDPI

Article

Numerical Investigation of the Performance of a Submersible Pump: Prediction of Recirculation, Vortex Formation, and Swirl Resulting from Off-Design Operating Conditions

Virgel M. Arocena, Binoe E. Abuan, Joseph Gerard T. Reyes, Paul L. Rodgers and Louis Angelo M. Danao *

Department of Mechanical Engineering, University of the Philippines Diliman, Quezon City 1101, Philippines; vmarocena@up.edu.ph (V.M.A.); beabuan@up.edu.ph (B.E.A.); jtreyes2@up.edu.ph (J.G.T.R.); paul112464@yahoo.com (P.L.R.)
* Correspondence: louisdanao@up.edu.ph

Abstract: Like any other turbomachinery, it is essential that the hydraulic behavior and performance of mixed-flow pumps are evaluated way in advance prior to manufacturing. Pump performance relies heavily on the proper design of the intake structure. Intake structures should be accurately designed in order to minimize and avoid unnecessary swirl and vortex formations. Ensuring the optimum performance condition as well as predicting how a particular intake structure affects the efficiency of the pump often requires either physical model studies or theoretical evaluations. Unfortunately, physical models are costly, time-consuming, and site-specific. Conversely, design and performance predictions using a theoretical approach merely gives performance values or parameters, which are usually unable to determine the root cause of poor pump performance. This study evaluates the viability of using Computational Fluid Dynamics (CFD) as an alternative tool for pump designers and engineers in evaluating pump performance. A procedure for conducting CFD simulations to verify pump characteristics such as head, efficiency, and flow as an aid for preliminary pump design is presented. Afterwards, a multiphase simulation using the VOF approach is applied to compare the fluid dynamics between four different pump intake structures. A full-sized CFD model of the pump sump complete with the pump's active components was used for the intake structure analysis in order to avoid scaling issues encountered during the reduced-scale physical model test. The results provided a clear illustration of the hydraulic phenomena and characteristic curves of the pump. A performance drop in terms of reduction in TDH was predicted across the various intake structure designs. The CFD simulation of intake structure provided a clear insight on the varying degree of swirl, flow circulation, and effect on pump efficiency between all four cases.

Keywords: mixed-flow pumps; CFD; performance; *Q-H*; intake structure; sumps

Citation: Arocena, V.M.; Abuan, B.E.; Reyes, J.G.T.; Rodgers, P.L.; Danao, L.A.M. Numerical Investigation of the Performance of a Submersible Pump: Prediction of Recirculation, Vortex Formation, and Swirl Resulting from Off-Design Operating Conditions. *Energies* **2021**, *14*, 5082. https://doi.org/10.3390/en14165082

Academic Editors: Michele Pinelli, Alessio Suman and Nicola Casari

Received: 16 July 2021
Accepted: 16 August 2021
Published: 18 August 2021

1. Introduction

A few of the specific hydraulic conditions that greatly affect the performance of any pump are swirl, vortices, and circulation. These are just some of the undesirable hydraulic phenomena that often lead to performance degradation, vibration, noise, structural damage, and even catastrophic failure. These phenomena are also highly influenced by flow conditions in the intake structure. Poorly designed intake structures are those that fail to control the possible harmful formation of swirls, free-surface vortices, and submerged vortices. These swirls and vortices can induce cavitation growth if not fully suppressed. Despite this fact, the proper design of these intake structures is amongst the most overlooked aspects when designing a pumping station.

Theoretical means of evaluating a pump's performance is a highly intensive process. Aside from the numerous geometric parameters involved, the hydraulic conditions present in any pump are complex, and the physics of which are not fully understood. It is for this reason that most pump engineers often rely on designs based on rule-of-thumb or standards

established from previously proven designs. This practice, along with some financial constraints, often limits design iteration and restricts the development of new products.

Most major hydraulic projects are model tested to optimize the design. For intake structure design, reduced-scale physical model tests had remained a primary mandatory requirement in keeping with existing codes and standards. ANSI/HI 9.8 [1] states that model tests shall be conducted when the sump geometry deviates from standardized designs, when approach flow is non-uniform or non-symmetric, or when the discharge rate is high (greater than 2.5 m^3/s per pump or 6 m^3/s per station). These tests provide design engineers with a visual image of what the flow will be during actual running conditions. They represent reality at a certain scale. Among the advantages in performing a physical model tests are that most parameters and operating boundaries involved are controllable, and the measurements, in general, are easy to perform. Unfortunately, aside from being expensive, site-specific, and time-consuming, results from physical model tests are highly influenced by scaling issues, incomplete modeling, and laboratory effects.

On the other hand, the implementation of Computational Fluid Dynamics (CFD) in fluid flow applications had grown in parallel with the advances in computer technology. CFD coupled with stress analysis had been actively used in the design of various pump components such as shafts, seals, impellers, diffusers, and casings, among others. For numerical studies, both the accuracy and robustness of the results vary heavily based on various turbulence parameters and modeling methodologies. Particularly for pump intake structure design, prediction of both free-surface and subsurface vortices using CFD had been a continuous focus. Constantinescu and Patel [2] were among the first to simulate the three-dimensional flow field on a simple water-intake bay. Their work solves the Reynolds-averaged Navier-Stokes equation with a two-layer k-ϵ turbulence model. The numerical solution was able to predict the expected vortex formation. However, it was emphasized that the resulting symmetric vortices caused by idealized flow conditions in the numerical solution are unlikely to exist in reality. These results were later verified by Rajendran and Patel [3] by constructing a 0.003 m^3/s rectangular pump sump model. Using particle-image velocimetry (PIV) to measure velocity fields, they were able to confirm that the previous CFD results for the position, number, and overall structure for both the free-surface and subsurface vortices were in good agreement with the physical model.

While there are numerous numerical and experimental studies concerning vortex prediction and flow phenomena in pump intake structures [4–6], most do not consider any impeller-induced flow. This is because most physical model experiments also do not include the impeller geometry in the scale model. Instead, a vertical pipe is used to represent the pump structure. Most studies only focus mainly on the flow condition upstream of the pump. One slight exception is the study made by Nagahara et al. [7]. In their study, they included the shape profile of the pump impeller and guidevane. They aimed to identify the relationship between the subsurface vortex strength and the size of the vapor cavity in the blades. The impeller remained stationary during the test, and no impeller-induced flow was considered. Instead, only the interaction between the vortex strength and the radial and axial forces on the blades were evaluated.

In factory test facilities, physical model studies, and even on existing numerical simulations, pump and intake structures are often evaluated separately. Constructing a test facility to verify the performance of the pump and sump prototype is not ideal for even the largest factory. Similarly, no specific code and test procedure are established in conducting a reduced-scale hydraulic model test that incorporates the pump geometry to the model. In this regard, this study presents a methodology to evaluate both pump and intake structure performance using CFD. To establish this, pump performance characteristics in terms of head, flow, and efficiency are first simulated. Then, flow dynamics, vortex prediction, and pump performance are conducted using a full-scale numerical model of the entire pump and intake structure. To analyze the effect of pump intake geometry, several intake structure designs are presented in order to compare the performance of each type. The

focus is on a method that would result in reduced computational efforts in order to merit its use as an engineering design tool.

2. Pump Performance Prediction

This section focuses on the CFD simulation of a mixed flow pump predicting various performance characteristics such as head, capacity, efficiency, and flow dynamics. The analysis aims to define through numerical simulation the performance curves of the mixed-flow pump, whose specifications are outlined in Table 1. The KSP-CV pump model is among the long-range of high-quality pumps manufactured by Tsuchiura Works, Machinery System Division of Hitachi, Ltd. These pumps are designed for various applications such as steelworks, industrial and chemical plants, irrigation, waterworks and sewage systems, power stations, and nuclear power plants. The KSP-CV pump used in this study is a single-stage vertical-shaft mixed flow submersible pump. These particular pump models have a typical head range between 3 m to 90 m and are designed for large-capacity operations. The active components for this pump are the rotating impeller and the stationary guidevane. The impeller has 5 blades and is rotating at N = 600 RPM, while the stationary guidevane has 12 vanes. The pump is driven by a 2500 kW motor, which proves that it is a high-energy pump. To protect proprietary information, only the basic data about the pump (i.e., Expected Performance Curves [8], Ratings) will be presented in this paper. The curves derived from the simulation for this pump will serve as the basis for the full-scale model analysis that will be presented in the succeeding sections of this study. In order to not exceed the available computational resources, disk friction losses, mechanical losses, leakage losses, and tip clearance effects are not included in this calculation. In addition, the walls were assumed to be smooth, and any disturbances due to surface roughness were neglected.

Table 1. Pump Specifications.

Specification	Value
Type Form	KSP-CV
Specific Speed [a]	83
Suction Bore (m)	1.257
Discharge Bore (m)	1.25
Stages	single
Capacity (m^3/h)	16,900
Total Dynamic Head (m)	39
NPSHa (m)	13
Speed (rpm)	600
Driver Type	motor-driven
Driver Rating (kW)	2500
Design Efficiency (%)	85
Service	CWP

[a] Dimensions are not used. Values shown are based on rate of flow at optimum efficiency in m^3/s, total head in m, and rotative speed in rpm.

2.1. Computational Domain

The computational domain includes the inlet or suction pipe, impeller, guidevane, column pipe, and 90° discharge elbow. The hexahedral meshing scheme is used for the whole domain. The 3D shape of the impeller was generated using ANSYS CFX-BladeGen, while the O-type grid was generated using ANSYS CFX-TurboGrid. The domain is separated into 4 regions in order to achieve a reasonable number of grid elements. The impeller and guidevane regions were modelled with a high-density mesh since these areas were expected to have a high solution gradient. The inlet pipe, column pipe, and discharge elbow regions, on the other hand, have lower density mesh count. The inlet pipe for this particular pump model incorporates four (4) 90° cross plates regulating pre-whirl and impeller backflow under partial flow conditions. This feature, together with the inlet extension, ensures that the flow is fully developed as it enters the domain. Similarly, the column pipe length is designed with enough length to prevent flow from recirculating back

to the guidevane. The front and rear cavities of the impeller were partially included in the control volume but with zero leakage flow rates. The 3D model and the mesh model of the mixed flow impeller and guidevane are shown in Figure 1. Similarly, a schematic of the whole computational domain, as well as the mesh for the whole assembly, is shown in Figure 2.

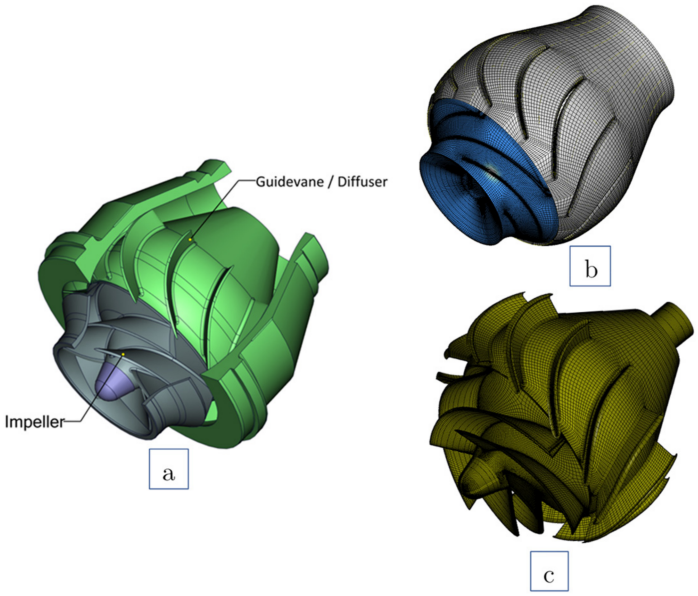

Figure 1. (**a**) The active components for the KSP-CV: 5-blade rotating impeller and 12-blade stationary guidevane/diffuser. (**b**) The generated hexahedral mesh used for the numerical analysis. (**c**) Impeller and guidevane blade walls.

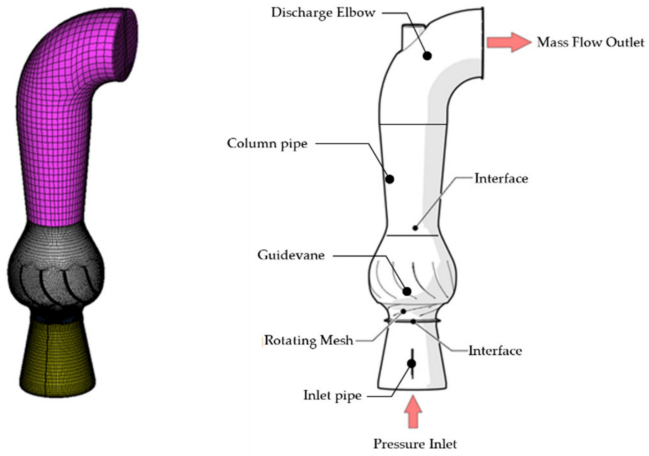

Figure 2. A schematic of the whole computational domain (**right**) and the mesh for the whole assembly (**left**).

2.2. Boundary Conditions and Solution Schemes

To solve the rotor-stator interaction problem in the domain, the multiple reference frame (MRF) approach is applied. The MRF approach is one of several models available in ANSYS Fluent in dealing with flows in systems containing translating or rotating components. For mixed flow pumps, all parts connected to the rotating shaft are moving with a certain angular velocity, while the other parts, such as the casing, guidevane, suction bell, etc., remain stationary. In general, the flows in such turbomachinery are unsteady in nature. This unsteadiness becomes even more apparent when viewed by a stationary observer. On the contrary, if viewed by an observer standing on the rotor, the flow would

appear to be in a steady state. Using this perspective, the MRF model treats an unsteady problem (with respect to the absolute reference frame) as a steady-state problem with respect to the moving reference frame. When using the MRF model, additional source terms such as centripetal and Coriolis acceleration are added to the equation of motion to account for the transformation from the stationary to the moving reference frame. Note that, during the analysis, the mesh is fixed or frozen on a specified position, and the instantaneous flow field is observed with the rotor in that position. It is because of this analogy that the MRF is often referred to as the "frozen rotor approach". Although this approach is clearly an approximation of steady-state conditions, the MRF model simplifies the problem and consequently requires less time and computational effort. For preliminary design and development, this makes the MRF approach an attractive model for industrial applications such as stirred tanks, wind turbines, fans, and other turbomachinery. For this study, the impeller region is assigned to a moving reference frame, while the rest of the region is assigned to a stationary frame. Calculations were carried out under single-phase, steady-state conditions with water at 25° C as the working medium. Flow is incompressible and isothermal with constant fluid properties. Turbulence was modeled using the Realizeable k-ε since it shows better agreement with pump test data as compared to the other two k-ε models (i.e., RNG and standard) [9]. A pressure-based coupled solver was applied. The second-order discretization scheme was used for pressure, momentum, density, and turbulence equations. Static pressure is defined at the inlet, while a mass flow rate was prescribed at the outlet. A 5% turbulent intensity was specified for the inlet, and the hydraulic diameter for both inlet and outlet was set equivalent to the respective pipe diameters. The flow was specified as subsonic, and all walls were treated as no-slip.

2.3. Grid Independence Study

To optimize the computational time and to study the effects of grid resolutions, a preliminary grid independence study at 90% rated flow was conducted to compare the results for three CFD models. The grid independence study ensures that the results are due to the boundary conditions and physics used and not the mesh resolution. Three hexahedral mapped meshed models were generated, with element counts of 0.9, 3.6, and 5.2 million cells to represent models with coarse, medium, and fine mesh, respectively. For the model used in this paper, the mesh refinement did not follow the usual half/double element size. This is because refining the mesh by a factor of 2 will result in an 8-fold increase in problem size and is unacceptable for engineering design purposes. Since the analysis is concerned with flow dynamics in the impeller and guidevane, the mesh variation for all three CFD models is focused on these two regions. There is no significant need to refine the mesh for the inlet pipe and discharge elbow because the velocity gradients in these areas are expected to be low. Likewise, knowledge of the flow patterns in these areas is not key in the analysis. Non-overlapping mesh interfaces were adapted in ANSYS Fluent to combine the four regions. The independence between areas with different mesh densities was improved by refining 2 to 3 mesh layers near the interface. A focused view of the coarse, medium, and fine meshed models are shown in Figure 3, while a tabulated data of the mesh count and the respective solution time using an 8-core 4.6 GHz Intel Core i7 9700 K desktop with 32 Gb of memory is shown in Table 2.

Table 2. The cell count for each region and simulation time.

	Coarse Mesh	Medium Mesh	Fine Mesh
Inlet Pipe	208,880	208,880	208,880
Impeller	374,300	2,994,400	2,994,400
Guidevane	317,160	317,160	2,537,280
Discharge Elbow	37,904	37,904	47,088
Total Cells	938,244	3,558,344	5,787,648
Solution Time	15 min	47 min	7 h. 8 min.

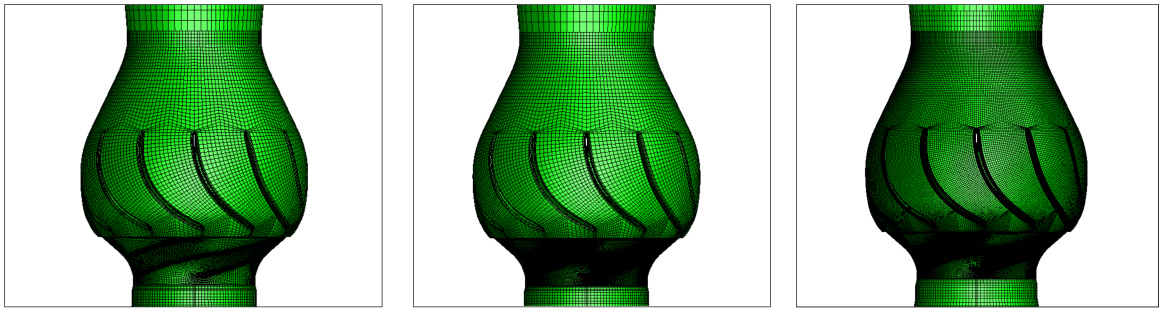

Figure 3. The mesh used for the grid independence study.

For all three numerical models, a steady-state simulation for the problem was conducted, where the mean velocity and the amplitude of the fluctuating field do not vary for more than 1% for each iteration. The target residual errors are kept below 10^{-4}. The pump head, as monitored throughout the entire calculation period, can be seen in Figure 4. For the three mesh densities, it can be hypothesized that the solution is very stable and that the calculated pump heads are nearly identical.

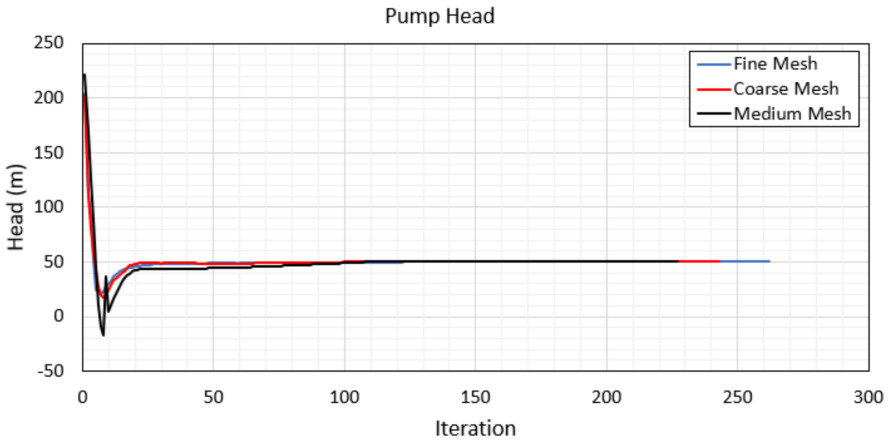

Figure 4. The pump head at 90% rated capacity as monitored during numerical simulation.

To qualitatively evaluate the grid independence, the axial velocity (z) at several points along a line just below the impeller eye and perpendicular to the flow direction is plotted, as shown in Figure 5. Additionally, in Figure 6, the total pressure contour on the center of the pump assembly is plotted for all three numerical models. Based on these figures, the simulation results show, in general, a close agreement between the three results. Specifically, for the velocity plots, a maximum variation of 1.4% was observed, particularly between the results for the fine mesh and the coarse mesh models. Additionally, the evaluation shows that even though the cell count for the medium mesh model is about 25% less than that of the fine mesh model and with a 90% reduction in calculation time, the difference in the results between these two models is almost negligible at 0.01%. The pressure distribution within the impeller and the guidevane regions on all three models are identical. The resemblance between the results from all three models shows that these simulations can be considered relatively grid-independent based on the presented mesh densities. Generally, for such cases, the coarse mesh is the best alternative for succeeding simulations in terms of minimizing computational time. However, in this paper, considering how close the results are between the fine mesh and the medium size mesh, and to more fully resolve the other phenomena of interest (e.g., vortex formation and air entrainment), the medium-sized mesh model was used.

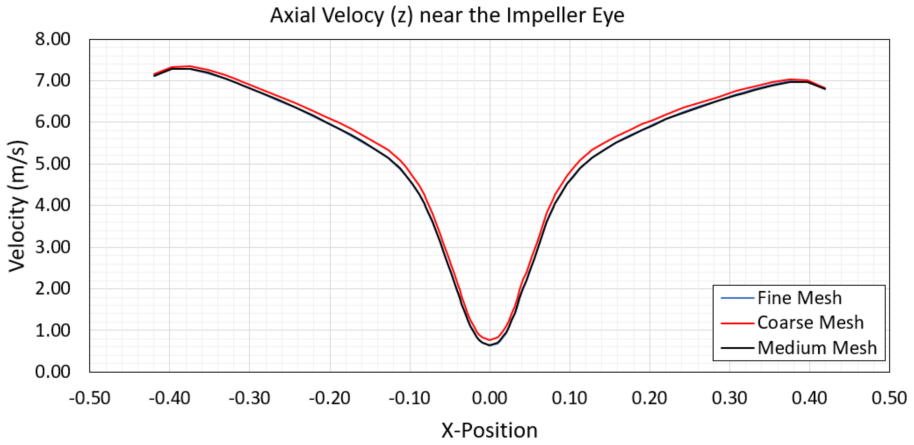

Figure 5. The axial velocity distribution near the impeller eye at 90% rated capacity.

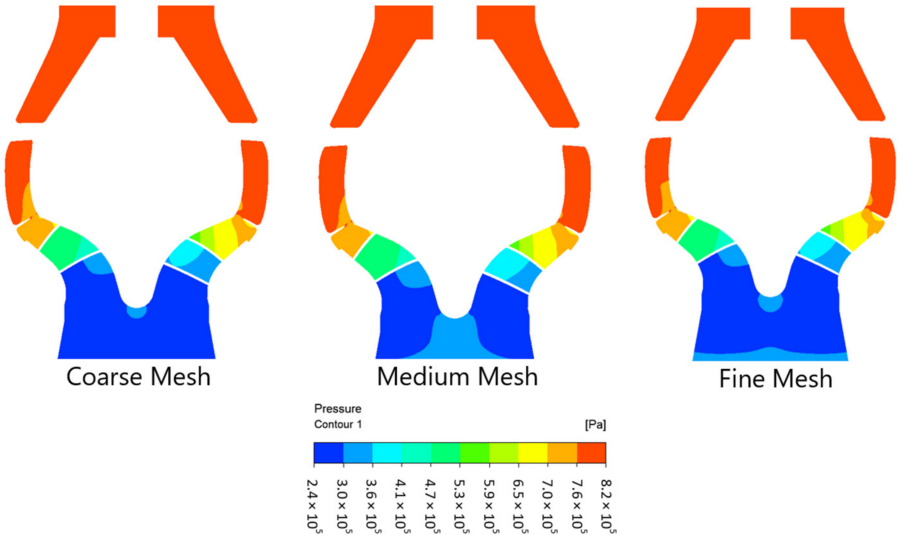

Figure 6. The pressure gradient across the pump assembly at 90% rated capacity.

3. Results and Discussions

Performance Curve

For the performance prediction, numerical simulations were performed from 10% to 150% of the nominal rated capacity with 10% increments, while shut-off (zero flow) may be interpolated. For all simulations, the rotor speed is kept constant at 600 RPM. The pump head, shaft power, and efficiency were calculated as follows:

$$\text{Head}: \; H = \frac{P_{out}}{\rho g} - \frac{P_{in}}{\rho g} + \Delta z, \tag{1}$$

$$\text{Shaft Power}: \; P = T \times \omega, \tag{2}$$

$$\text{Efficiency}: \; \eta = \frac{\rho g Q H}{P}, \tag{3}$$

wherein P_{in}, P_{out} are the area weighted average of the total pressure taken at a cross-section at the pipe inlet and at the end of the pipe column (just before entering the discharge elbow), respectively. Q is the fluid flow rate, g the acceleration due to gravity, and ρ is the fluid density. The tabulated results for all analysis points are shown in Table 3. Figure 7 shows the graph of the numerical results for the head, efficiency, and power as a function of the flow rate superimposed on the expected pump performance curve as provided by the manufacturer [8]. It can be seen from this figure that all three parameters follow a

consistent trend as compared with the manufacturer's data. This further shows that for this particular pump, doing the grid independence study at only one flow condition, for this case at 90% rated flow, is enough to consider the flow relatively grid-independent.

Table 3. Tabulated performance results for mixed-flow pump at 600 RPM.

Flow Rate (m^3/h)	Shaft Power (kW)	Pump Head (m)	Efficiency (%)
1519	2288	78	14
3038	2260	75	27
4556	2118	70	41
6075	2007	65	54
7594	1963	62	66
9113	2080	62	74
10,632	2164	60	80
12,151	2230	57	85
13,669	2285	54	88
15,188	2328	50	89
16,707	2318	45	89
18,226	2262	39	87
19,745	2163	33	82
21,264	2017	25	71
22,782	1824	16	54

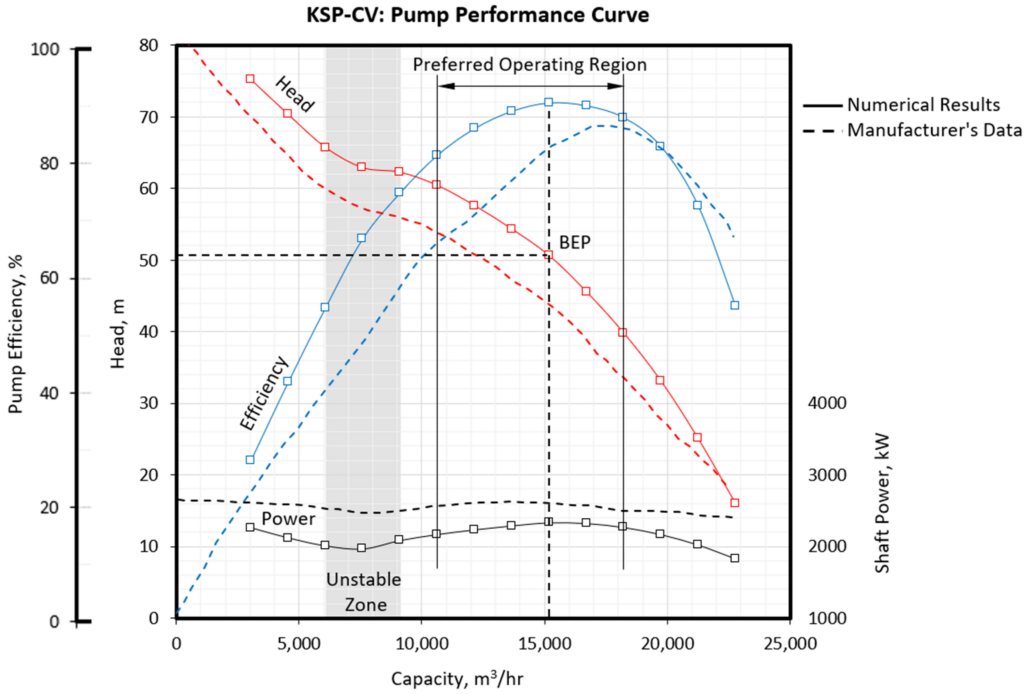

Figure 7. The pump performance curve based on numerical results as compared with the expected performance curve acquired from the manufacturer [8].

Based on the relationship between the head, flow rate, power, and pump efficiency (Figure 7), it can be seen that the power requirement is much flatter and does not vary too much along the pump's operating range. This type of characteristic curve is typical of the mixed-flow pump and is, in turn, different from those of radial-type pumps, where a larger flow requires higher power. This is because of the very large area of flow against the comparatively small impeller diameter in axial and mixed flow pumps. Hydraulics performance, however, differs appreciably, and the head capacity (*Q*-*H*) curve tends to be steep, with the point of maximum efficiency shifted towards maximum capacity. This

characteristic can be verified in the chart where the best efficiency point (BEP) is located at high flow rates as expected.

Figure 8 shows the flow pattern and pressure distribution when operating the pump at Q_{BEP}. It can be seen that at Q_{BEP}, flow is perfectly aligned with the blade profile. However, it is evident that the leading edge of the blade acts as an obstruction for incoming flow, creating an area having a low static pressure on both sides of the blades. This shows that even at the best efficiency point where the flow direction is perfectly aligned with the blade, cavitation can still take place once there is a significant drop in the inlet pressure. Specifically, for the pump in this study, it can be assumed based on the same figure that because of the lower pressure, cavitation will most likely start to form on the suction side of the blade.

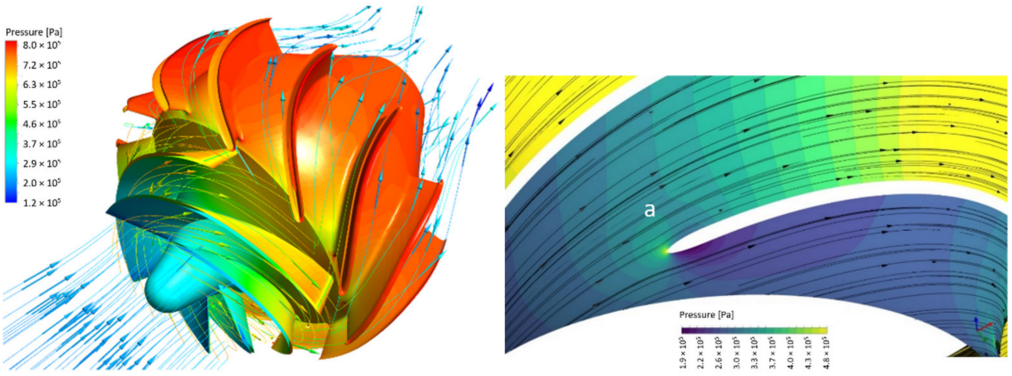

Figure 8. Velocity streamlines and pressure distribution at Q_{BEP}. Even when flow direction is perfectly aligned with the blade, the blockage effect (a) still exists on the blade tip causing a decrease in pressure on both sides of the impeller blade.

All rotodynamic vertical pumps have limitations on the minimum flow at which they should be operated continuously or for an extended period of time. For specialized high energy pumps, flow limitations may be set as high as 70% of Q_{BEP}, while for low energy pumps, the allowable flow may be set as low as 20% of Q_{BEP} [10]. These flow limitations vary across various manufacturers and depend heavily on the type of application and impeller design. The next two figures show the flow pattern inside the pump when it is operated within the unstable region.

In Figure 9, it can be seen that at the rate of flow equivalent to 50% of Q_{BEP}, the fluid tends to return from the guidevane back towards the impeller. This phenomenon is called discharge recirculation, which primarily occurs during part-load or at low capacities. Recirculation often results in strong noise, vibration, and rotor stall. Further reduction in flow beyond the unstable region (30% of Q_{BEP}) will cause recirculation to shift towards the suction side of the impeller, forming a vortex region between the impeller blades, as shown in Figure 10. This low-pressure area can lead to cavitation accompanied by intense pressure pulsations which ultimately damages the impeller because of the undue stress to the rotor components. Additionally, Alpan and Peng [11] reported that fluid recirculation in the suction nozzle (suction recirculation) is the main source of power loss at low flow rates.

Generally, the effect of recirculation is still questionable and sometimes trivial at best. In some applications, recirculation is a constructive phenomenon and may even be advantageous to the design (e.g., regenerative pumps). In these cases, a desirable effect of recirculation is to have the same (recirculating) volume of fluid to be acted upon by the impeller multiple times, thereby increasing fluid energy. Therefore, it is easy to conclude that recirculation can contribute towards higher heads compared to conditions without recirculation. However, there are also some instances where recirculation can lead to an unfavorable dip in the *Q-H* curve (Figure 7). At least for the mixed flow pumps covered in this study, recirculation is an unfavorable phenomenon, and the additional head caused by recirculation is meaningless since mixed-flow pumps cannot operate in these regions. Operating at such low flows will cause these types of pumps to experience full cavitation.

Based on the results of the CFD analysis, for this pump, it can be concluded that continuous operation below 60% of Q_{BEP} should be avoided.

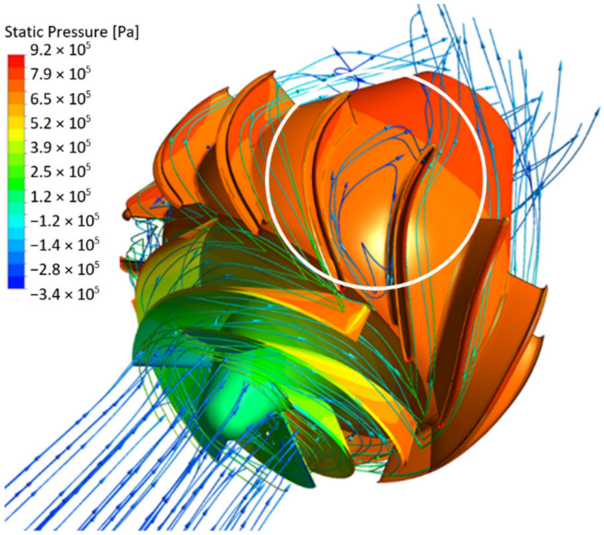

Figure 9. Discharge recirculation at a flow equivalent to 50% of QBEP. The fluid tends to recirculate from the guidevane back to the impeller. This circulatory flow can cause large forces on the impeller shrouds resulting in unbalanced axial forces and high thrust.

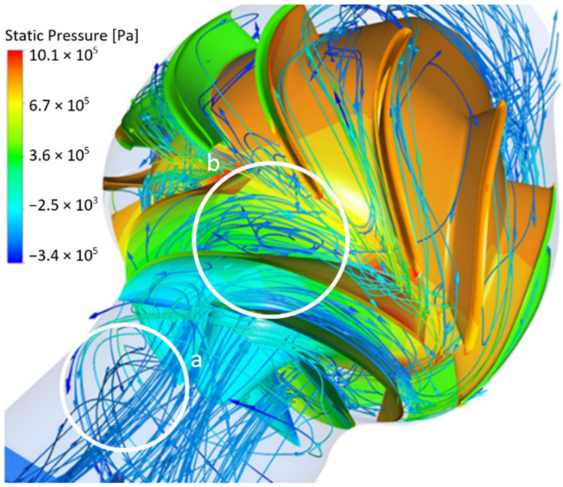

Figure 10. Suction recirculation at 30% of QBEP. The pump operating at this reduced flow causes the flow to separate from the blade and circulate back upstream, and in this case, even back to the suction pipe. Undesirable phenomena such as eddies and pre-rotation are observed to form within the inlet pipe (a) as well as strong, high-velocity vortices between the impeller blades (b).

The MRF mesh calculations led to some overprediction of the head as compared to the expected pump performance data. The overprediction increases with decreasing flow rate. This is primarily due to the leakage flow in the pump, which was not accounted for in the present calculations since the gap between the impeller and the labyrinth seal is considered non-existent. Applying the necessary correction for leakage losses would certainly bring the calculated results close to the manufacturer's data.

If the overprediction is to be disregarded or considered acceptable, these results would mean that the published rated capacity of 16,900 m^3/h and TDH of 39 m, as previously shown in Table 1, is 10% above the BEP.

4. Full-Size Pump Sump Numerical Analysis

Numerous design suggestions and guidelines regarding reliable optimal intake structures can be found in various pump standards, such as those published by the Hydraulic Institute [1] and the British Hydromechanics Research Association. Ideally, pump sumps should be simple and easy to construct. Although it is not always possible to build an intake structure that conforms to these guidelines. In certain cases, space and cost limitations are a primary concern. Conversely, in others, such as during site rehabilitation, replacing an aging pump with a new one poses a daunting challenge, especially because hydraulic conditions on the existing sump are unknown.

4.1. Sump Geometry Variations

Figure 11a represents the geometry of the rectangular sump, which served as the baseline for the analysis (Case 1). All dimensions are according to recommendations set by the Hydraulic Institute [1]. No splitters, fillet, curtain wall, or any form of anti-vortex device was installed in order to obtain a clear baseline result. ANSI/HI 9.8 [1] outlines the recommended dimensions for a rectangular sump, but oftentimes, due to site-specific flow conditions, additional modifications are necessary. This is to prevent any vortex formation that could affect the performance of the pump. In such cases, various pump publications outline design recommendations that aim to aid engineers in selecting the proper design. Some designers prefer to further modify this design by providing the sump with two semi-circular walls. With the notion that this would eliminate the vortices that appear in the corners of the sump. In practice, the advantage of this modification is trivial. In fact, some installations have experienced vortices along the center of the semicircles. Nearer the suction pipe as compared to sumps with corner vortices. For this study, a variation of this design is presented in Figure 11b (Case 2), wherein a floor cone and splitter are added in order to try to alleviate the side effect mentioned above.

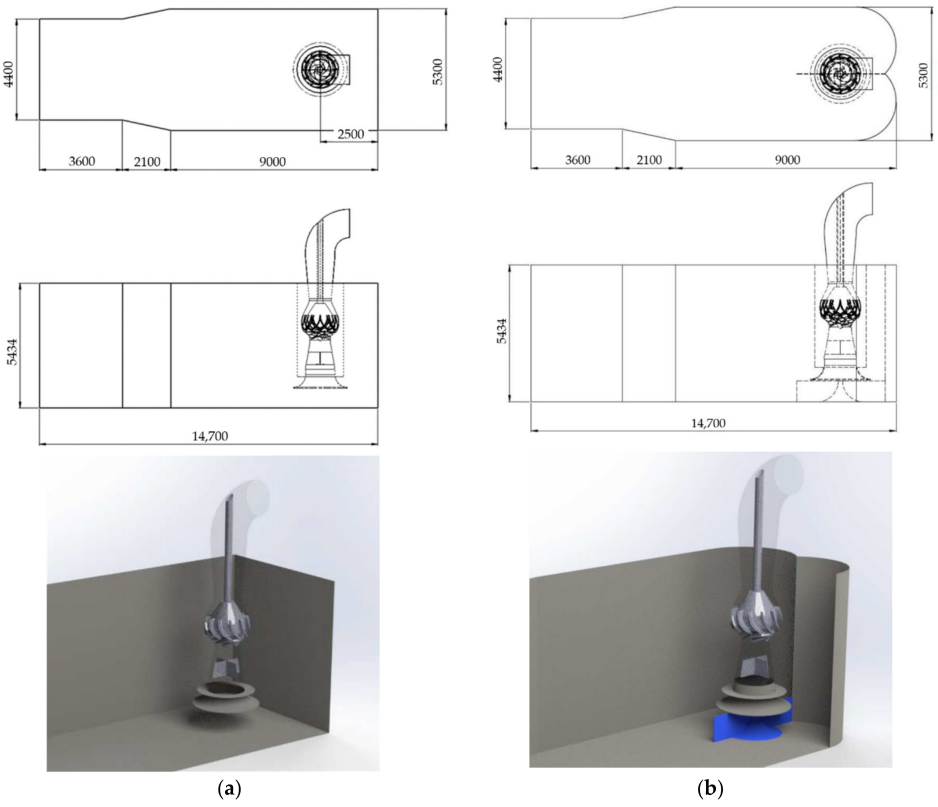

Figure 11. (**a**) A rectangular pump sump model with mixed-flow pump and guidevane (Case 1); (**b**) a pump sump utilizing semicircular arches as a backwall (Case 2). In addition, a floor cone and a splitter are installed to prevent floor sub-surface vortices.

Another popular variation on the recommended sump design is one proposed by Ingersoll-Rand [12]. Their proposed design uses tetrahedral floor splitters instead of the conventional fillet. A slight variation on the design, as shown in Figure 12a (Case 3), was used as the third model for this study. For this model, the central floor splitter was replaced with a floor cone and plate combination in order to increase the area underneath the bellmouth. The aim is to reduce the head loss observed in the unmodified sump (Case 1). Lastly, Figure 12b shows a formed suction intake (FSI) structure used for stations with adverse inflow conditions. It is said that these designs are relatively insensitive to the direction of approach and skewed velocity distribution at the suction bell mouth. Such configurations are usually used where it is difficult to design standard inlet structures due to space limitations. An advantage that an FSI has is that it can normalize any erratic or swirling flow by re-directing the flow vertically into the pump impeller. The increase in the fluid's velocity as it enters the FSI reduces the sump's susceptibility for sub-surface vortex formation. The FSI model presented in this study (Case 4) is a variation of the "TYPE 10" FSI design developed from the results of the research conducted by the US Army Engineer Waterways Experiment Station (WES). Specifications for FSI types 1 and 10 can be seen in USACE engineering and design manual EM 1110-2-3105 [13], referencing ETL 1110-2-327.

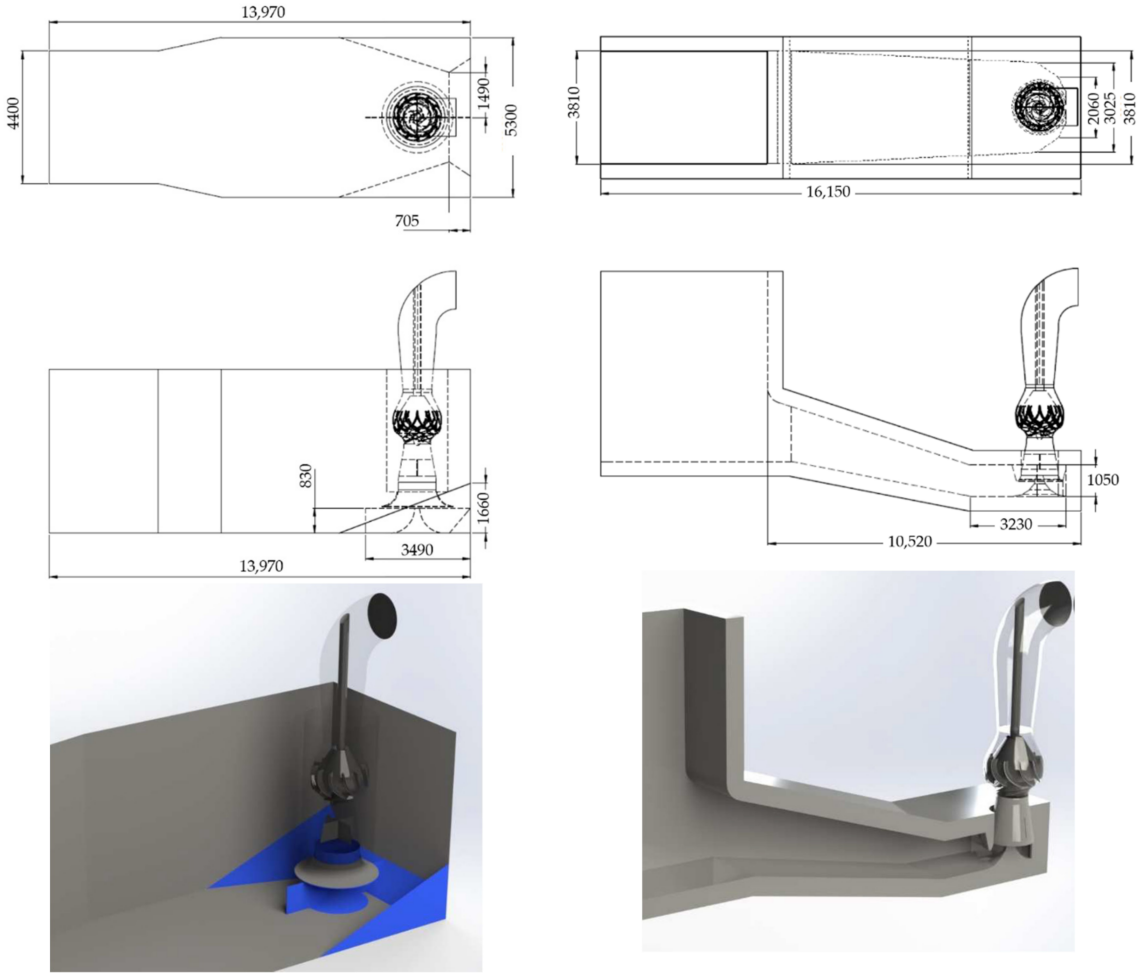

Figure 12. (**a**) A variation of the pump sump based on Ingersoll-Rand (1991) recommendation using a floor cone instead of a floor splitter (Case 3), (**b**) A variation of a forced suction intake (FSI) model pump sump based on the "TYPE 10" FSI design developed by the US Army Corps of Engineers (ETL No. 1110-2-327) (Case 4).

4.2. Computational Domain and Boundary Conditions

For all the cases, the geometry and mesh were created using an in-house pre-processing software CADAS, and the numerical simulations were run using ANSYS Fluent. Similar approaches and methodologies with those discussed in Arocena et al. [14] are used throughout this section. Grid size and element lengths for Cases 1, 2, and 3 were derived from the grid independence study conducted on Case 1 of the same publication. The pump sump is modelled using a high-resolution hexahedral mapped mesh near the pump bellmouth (pump bay) and a coarser mesh upstream of the pump (forebay). The mesh of the pump used in the analysis in the previous sections is then added to complete the model. Figure 13 shows an overview of the mesh scheme for all four cases, with each hydraulic zone represented by a different color. All boundary conditions were calculated based on the rated capacity of 16,700 m^3/h, which is about 110% of Q_{BEP} and with a low water level (LWL) of 5.484 m. A velocity flow inlet with negative velocity magnitude (outflow) was prescribed as outlet boundary condition at the end of the discharge pipe, while the rectangular section serving as the entry point for the sump was prescribed as a pressure inlet boundary condition. The boundary condition for the air surface 2 m over the water surface was also specified as pressure outlet boundary with zero backflow volume fraction. Indicating that only air can pass through this boundary.

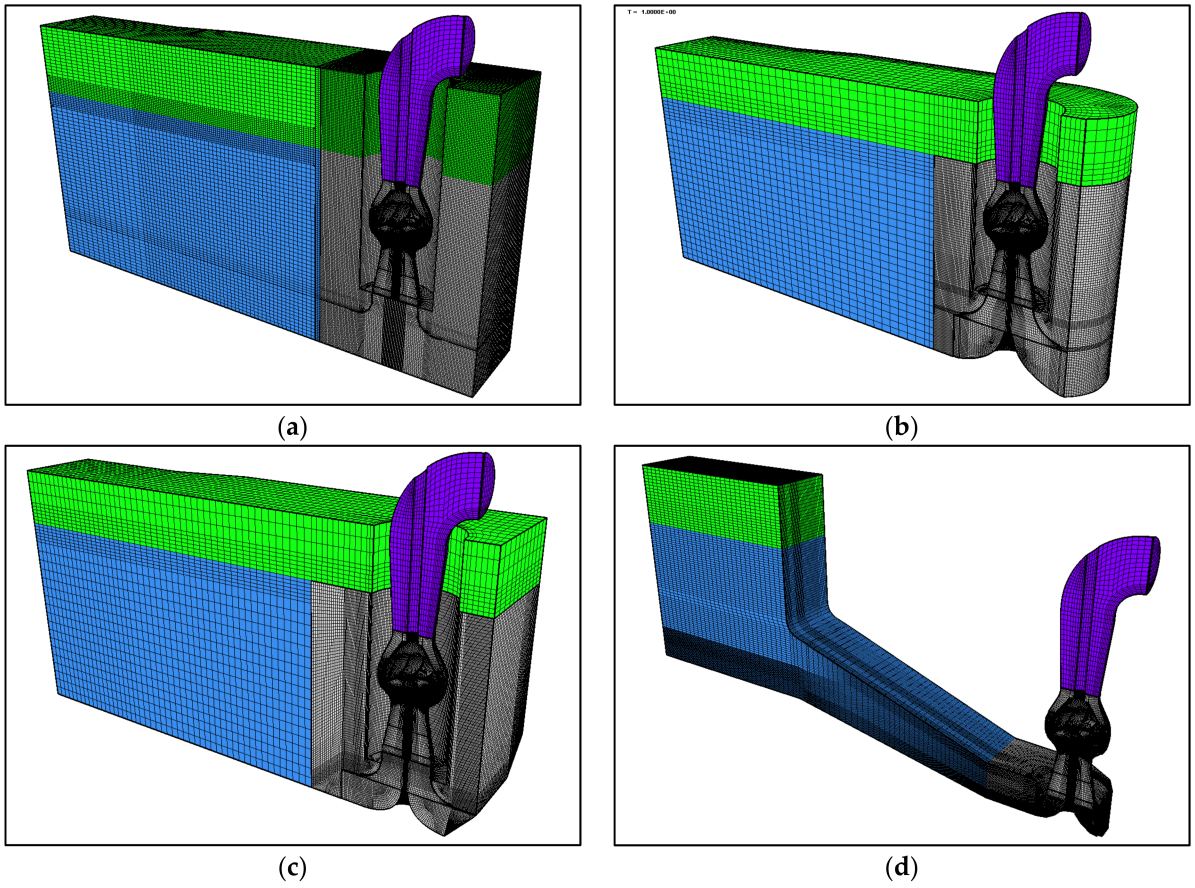

Figure 13. A cross-sectional view of meshed geometries for the 4 sump models: (**a**) Case 1, (**b**) Case 2, (**c**) Case 3, and (**d**) Case 4. Each model was separated into regions where high-density mesh count is created for regions with high velocity gradients.

At this point, it is important to highlight that the forebay for Case 1 represents the full-scale prototype for the reduced-scaled sump used in the physical model test presented in [14]. As an overview, it should be noted that for open channel flow, gravity and inertial forces play a more dominant role than viscous or turbulent shear forces. Keeping the

Froude number in both the model and the prototype constant is a good approximation of dynamic similitude [15]. As such, the 1:10 undistorted scale selected for the physical model test in [14] is based on a constant Froude number ($Fr = 0.38$) as computed across the suction bell for both the model and the prototype. Additionally, it was verified that the Reynolds number ($Re = 1.44 \times 10^5$) across the 260 mm diameter suction bell of the model is way above the minimum criteria of 6×10^4 as set by ANSI/HI [1]. This ensures that any scale effects will be minimized and that the flow in the model will be as turbulent as that of the prototype.

From the results of the physical model test, it can be expected that the selected forebay length for the numerical model is sufficient in providing a stable velocity gradient from the inlet of the domain. For pump intake structures, this stable approach flow is important in order to prevent any unnecessary turbulence, which could influence any free surface or subsurface vortex formation downstream of the forebay.

To solve the rotor-stator interaction problem in the domain, the multiple reference frame (MRF) scheme is applied to the domain. The impeller region is assigned to a moving reference frame, while the rest of the region is assigned to a stationary frame. Calculations were carried out under multiphase VOF transient conditions with water at 25 °C as the secondary phase and air as the primary phase. Turbulence was modelled using the k-ω shear stress transport (SST). SST *k*-ω had been found to be suitable for numerical modelling of free-surface vortices [16,17]. This turbulence model exhibits better performance in predicting flows at walls and adverse pressure gradients as compared to other eddy-viscosity models [18]. The transient formulation is second-order implicit. The converged solution from a steady-state simulation was used for the initial conditions.

5. Results and Discussions

Isosurface plots and surface streamline plots for the first three cases (Figure 14a–c) show no free-surface vortex formation stronger than type 2 (ARL's classification [19]) near the pump compartment. Cases 1 and 2 show type 1 (surface swirl) to type 2 (surface dimple) on the free surface of the water. As discussed earlier, the semicircular arcs added to the backwall magnified the surface swirl and directed the swirl nearer the pump column. If the semicircular arcs were constructed from two corner fillets instead of the current design, these surface swirls would have developed into full type 3 or type 4 dye core vortices. Instead, the sharp intersection of the two semicircular arcs served as a vertical backwall splitter that prevented any surface swirl from organizing and developing to a much stronger surface vortex.

For Case 1, strong type 2 (dye core) vortices attached to the sidewall and the sump floor were observed as the fluid began to separate from the wall and flow towards the bellmouth (Figure 14a). In contrast, for Case 2 and Case 3, there were no flow separation and the fluid remain attached to the fillets and splitters. This indicates that aside from using the recommended sump dimensions as published in various pump standards, it is still more advisable to check and minimize any sharp corners where eddies or dead zones would occur. The floor cone was effective in eliminating the floor vortex, but care should be given to not restrict the area under the bell too much that it would result in the pump experiencing additional head loss.

Although formed structure intakes (Case 4) are generally less sensitive to adverse inlet flow conditions, poorly designed FSI structures may still suffer from surface vortices in the forebay and subsurface vortices near the FSI channel. Particularly for Case 4, swirl and recirculation in the forebay area can be observed from the streamlines in Figure 14d. Large surface swirl/depression can be observed on the free surface area of the forebay. These are weak vortices whose cores do not reach the pump. Such phenomena can be avoided by the installation of curtain walls upstream. For FSI, however, such vortices, if left unchecked, can cause catastrophic damage to the structure. Noise, cavitation, and structural damage are among the most common results of such phenomena for these types of structures. Additionally, air-entrained pockets were observed, causing dispersed

air bubbles to constantly reach the intake bellmouth. This can be attributed to the same swirling action on the surface of the forebay.

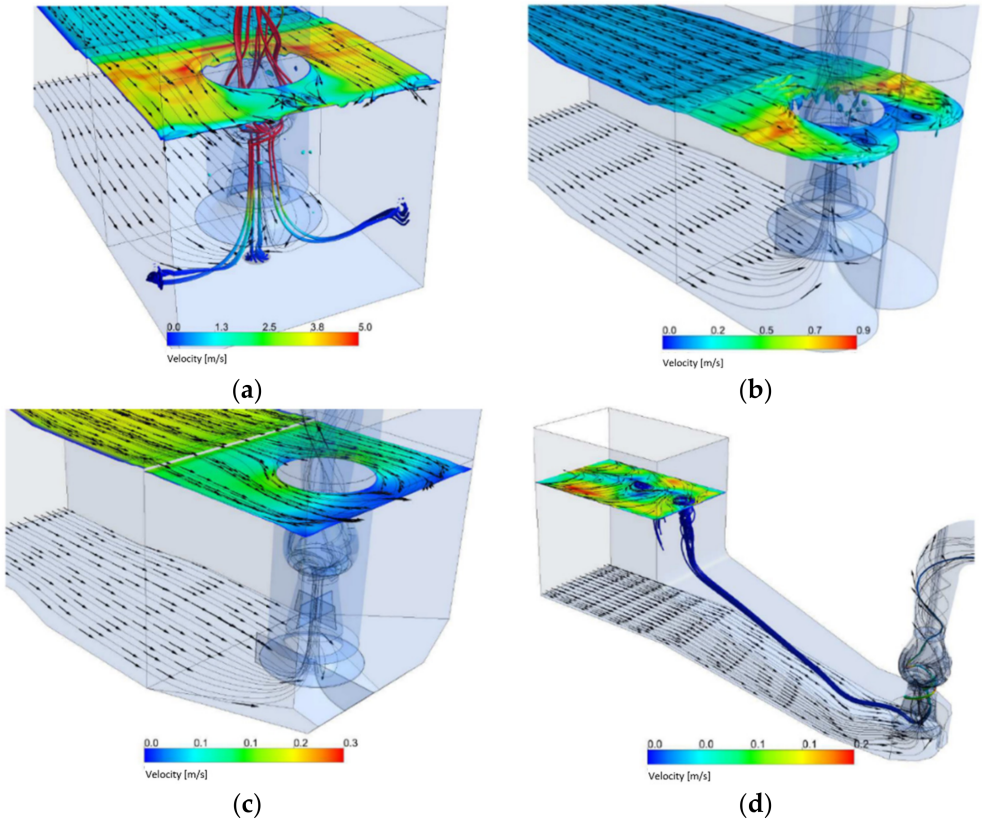

Figure 14. Plot of volume fraction isosurface with velocity contour overlay, approach flow streamlines, and vortex streamline: (**a**) case 1, (**b**) case 2, (**c**) case 3, and (**d**) case 4.

The CFD results (Figure 15) showed that for Cases 1 to 3, the swirl angles at the impeller eye are well within the 5° acceptance criteria for the short-term 30-s maximum set by ANSI/HI [1]. For these two cases, the average swirl angle was around 3.5°, while Case 2 showed a slightly higher average swirl of 3.8°. This negligible difference may be attributed to the slight turbulence present at the backwall for Case 2 caused by the semicircular arcs. Case 4 showed a very high swirl angle with an average of 10.1, which exceeds the maximum allowable value. This is in part due to the high fluid rotation as water enters the bell. The protrusions made by the floor cone (Figure 12b) into the bellmouth caused the fluid to rotate excessively as it enters the pump. This phenomenon caused additional issues such as uneven velocity distribution (Figure 16d), which usually results in unbalanced loading at the impeller shaft. Conversely, Figure 16a–c shows uniform velocity distribution for the first three cases.

Figure 17 shows point velocities as measured from the intake bellmouth throat. Cases 1–3 all show acceptable conditions based on ANSI/HI [1] criteria. The improvement in the velocity variation can be clearly seen across the three cases, with Case 3 having the most stable plot with a standard deviation of 0.1. On the other hand, Case 4 showed a large variation in point velocity again, proving that the flow is highly turbulent as the fluid enters the bellmouth.

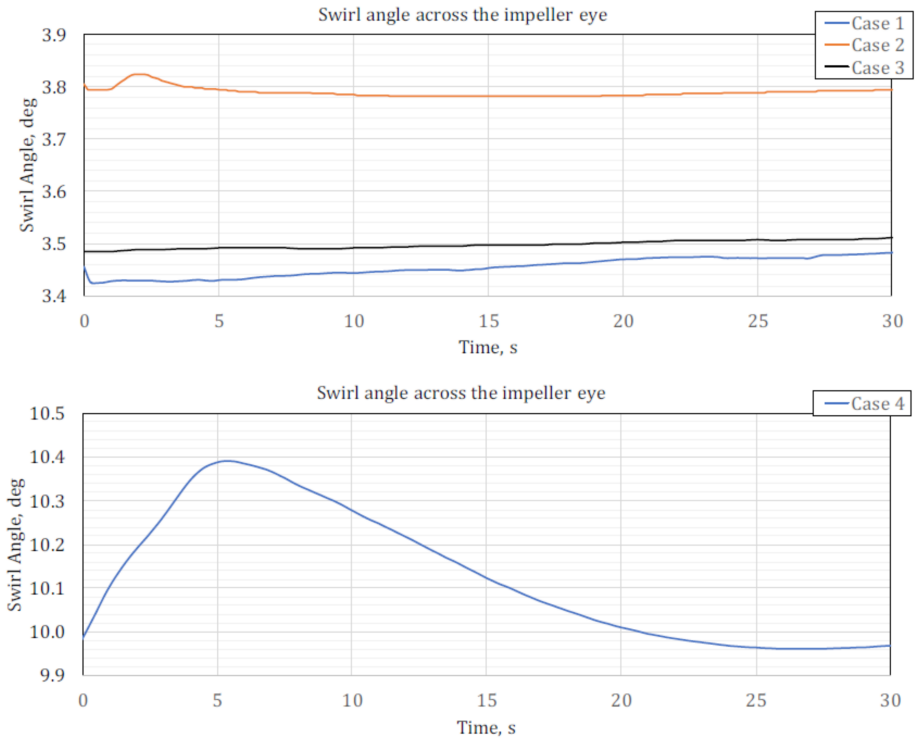

Figure 15. Swirl angle across the impeller.

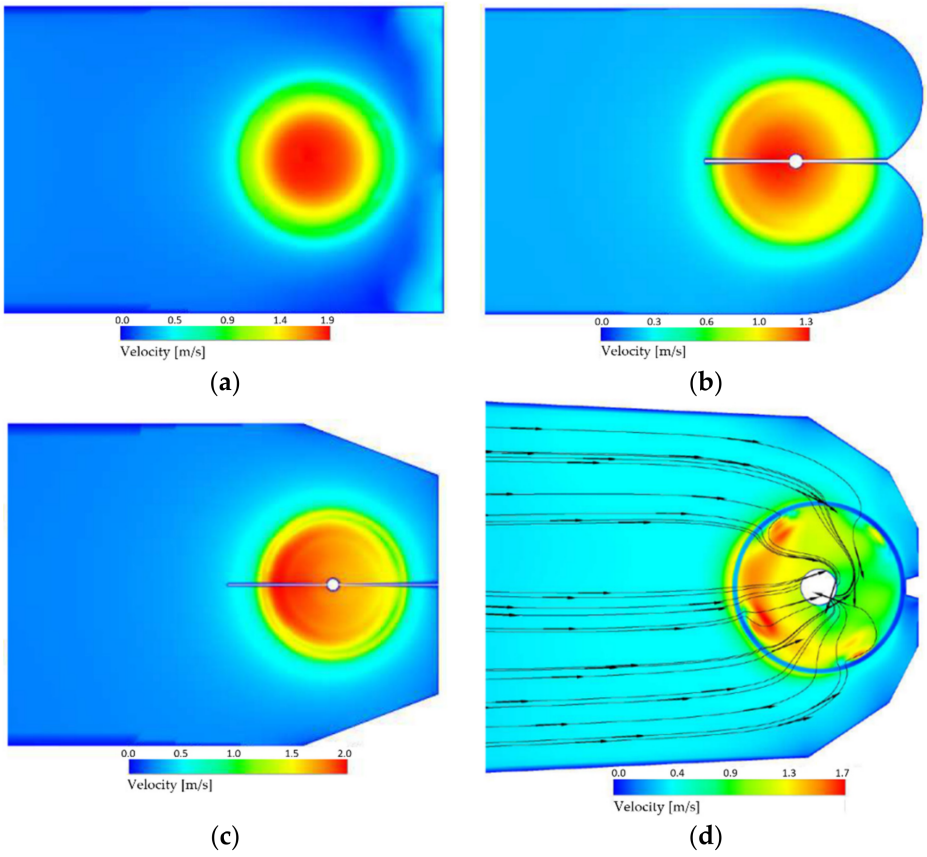

Figure 16. Velocity distribution at the suction bellmouth for all test cases: (**a**) case 1, (**b**) case 2, (**c**) case 3, (**d**) case 4. Notice the uneven velocity distribution for case 4.

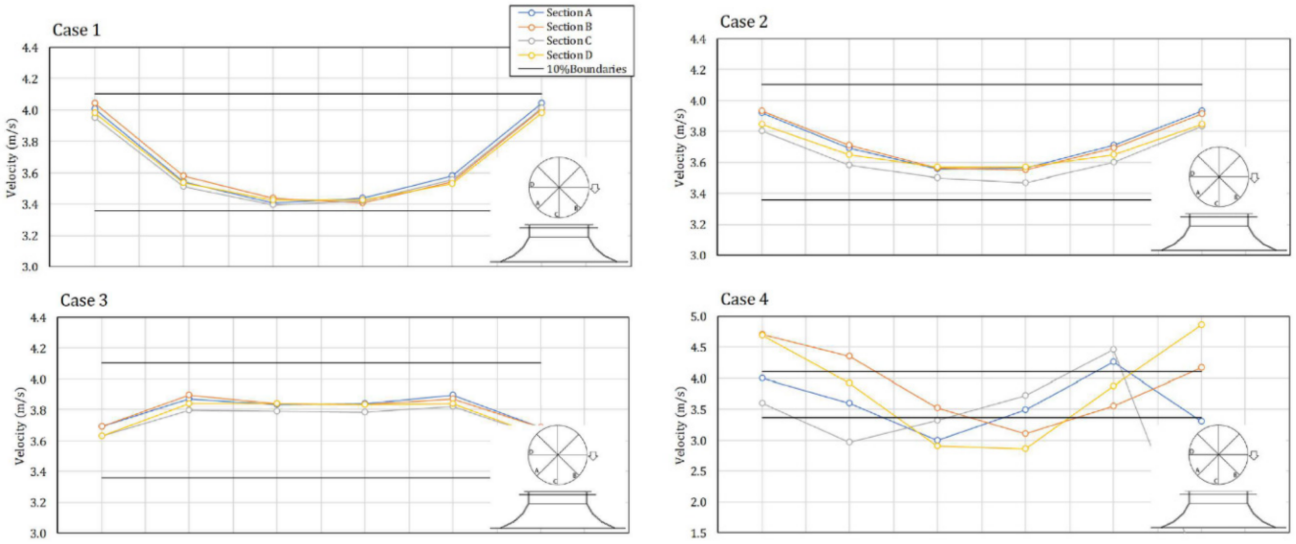

Figure 17. Point velocities at bellmouth throat.

An evaluation of the pump's performance for all the three cases, as shown in Table 4, further verifies that Case 3 presents the best hydraulic condition providing about 1% efficiency gain from the baseline geometry. Additionally, the table shows that although Case 2 was able to prevent the formation of subsurface vortices, the pump's efficiency suffered by 1% from baseline. This is due to the condition that swirl is higher in Case 2 as compared to the other two cases. This high swirl, as mentioned previously, may be attributed to the circulation at the back of the pump.

Table 4. Pump performance as installed in different sump geometries.

Case No.	Shaft Power (kW)	Pump Head (m)	Efficiency (%)
1	2165	37.4	78.6
2	2219	37.7	77.5
3	2196	38.2	79.3
4	2164	64.2	-

For the FSI model, CFD results showed a very high head. This is caused by the recirculation created by the excessive swirl at the intake of the pump, as shown in Figure 18. This increase in the head is primarily caused by having the same (recirculating) volume of fluid being acted upon by the impeller multiple times, thereby increasing fluid energy. This is desirable for regenerative pumps but not in mixed-flow pumps since, for Case 4, the pump would suffer severe cavitation.

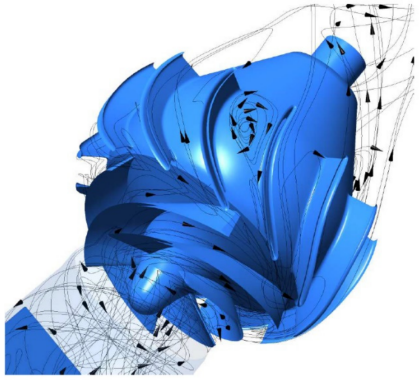

Figure 18. Suction and discharge recirculation caused by excessive swirl at the pump inlet bellmouth.

6. Conclusions

This paper presented numerical solutions to investigate the hydraulic performance of mixed flow submersible pumps under varying pump intake geometry and conditions. The focus of the paper is to develop a suitable method for setting up a numerical model and simulation procedure that could be utilized as an engineering tool during product development. To achieve this, the analysis should provide a balance between numerical accuracy and the efficient use of computational resources. In this study, a numerical model of the pump was used to establish the pump performance characteristics. Head, flow, and efficiency were compared to data provided by the pump manufacturer. Afterwards, CFD simulations of a full-scale pump and intake structure were conducted to predict the formation of free-surface and submerged vortices during operation. Several cases were presented in order to compare the effect of various geometries and vortex splitters on pump performance. The models were created in full-scale so as to avoid the scaling effects normally encountered during reduced-scale physical model tests. The results showed suitable accuracy in predicting the flow dynamics, intake structure performance, and pump characteristic curves.

From this study, it can be implied that significant room for improvements in terms of increasing accuracy of the results can easily be achieved through the inclusion of disk friction losses, mechanical losses, leakage losses, and the tip clearance effect, which were previously neglected in this study. The grid independence study made in this paper as conducted at only one flow condition, for this case at 90% of Q_{BEP}, is proven to be sufficient since the CFD results for the pump's characteristic curve were able to closely match the supplied performance curve. Conversely, if calculations show significant deviation from expected data, then it is strongly advised that the user conduct additional grid independence studies, particularly at flows where unsteadiness and circulation are apparent.

Additionally, note that although the MRF approach has found use in various industrial applications, this approach, being the simplest, is a steady-state approximation in which individual cell zones move at different rotational and/or translational speeds [20]. For purposes of product development and preliminary design, the MRF approach can provide reasonable insight into the flow. For turbomachinery applications with strong rotor-stator interaction or where large transient effects are expected, a more robust solution such as the sliding mesh model should be considered.

On the other hand, it was observed that CFD could provide results within a shorter period of time with a lower financial impact. Operating parameters, such as suction pressure, rotational speed, and fluid density, can easily be modified to verify pump performance under such loads. Additionally, through CFD, the ease of conducting geometric and parametric revisions, such as the number of blades, impeller attack angle, and impeller diameter on the numerical model, can provide pump designers with enough insight on the effect of these parameters, aiding in developing more efficient and reliable pumps. Various factors can still be developed to obtain more accurate results, such as consideration of cavitation growth in unsteady flow to analyze noise, vibration, and flow instabilities. However, for the purposes of this study, CFD may prove to be a viable option in developing optimum pumps, thereby reducing the need for extensive physical model experiments.

Author Contributions: Conceptualization, V.M.A.; methodology, V.M.A. and L.A.M.D.; software, V.M.A., B.E.A. and L.A.M.D.; validation, V.M.A. and L.A.M.D.; formal analysis, V.M.A. and L.A.M.D.; investigation, V.M.A.; resources, V.M.A.; data curation, B.E.A., P.L.R. and J.G.T.R.; writing—original draft preparation, V.M.A. and L.A.M.D.; writing—review and editing, B.E.A., P.L.R. and J.G.T.R.; visualization, V.M.A. and L.A.M.D.; supervision, B.E.A., P.L.R., J.G.T.R. and L.A.M.D.; funding acquisition, L.A.M.D. All authors have read and agreed to the published version of the manuscript.

Funding: This research was funded by the Department of Science and Technology (DOST) through the Engineering Research and Development for Technology (ERDT) Program—Local Graduate Scholarships. The APC was funded by DOST-ERDT Faculty Research Dissemination Grant.

Acknowledgments: The authors would like to thank Hitachi Plant Technologies, Ltd., Philippine Branch Office for granting permission to use the pump physical model test data and pump performance data presented as well as the meshing software used in this paper.

Conflicts of Interest: The authors declare no conflict of interest.

References

1. American National Standard. *Pump Intake Design*; ANSI/HI 9.8-1998; Hydraulic Institute: Parsippany, NJ, USA, 2012.
2. Constantinescu, G.; Patel, V. Numerical Model for Simulation of Pump-Intake Flow and Vortices. *J. Hydraul. Eng.* **1998**, *124*, 123–134. [CrossRef]
3. Rajendran, V.P.; Constantinescu, G.S.; Patel, V.C. Experimental Validation of Numerical Model of Flow in Pump-Intake Bays. *J. Hydraul. Eng.* **1999**, *125*, 1119–1125. [CrossRef]
4. Okamura, T.; Kamemoto, K.; Matsui, J. CFD Prediction and model Experiment on Suction Vortices in pump sump. In Proceedings of the 9th Asian Conference on Fluid Machinery, Jeju, Korea, 16–19 October 2007; pp. 1–10.
5. Rajendran, V.P.; Patel, V.C. *Patel, Characterization of Vortices in Model Pump-Bay Using Particle Image Velocimetry*; IIHR Technical Report No. 396; University of Iowa: Iowa City, IA, USA, 1998.
6. Lai, Y.G.; Weber, L.J.; Patel, V.C. A non-hydrostatic three-dimensional numerical model for hydraulic flow simulation-Part II: Validation and application. *J. Hydraul. Eng.* **2003**, *129*, 206–214. [CrossRef]
7. Nagaha, T.; Sato, T.; Kawabata, S.; Okamura, T. Effect of submerged vortex cavitation in pump suction intakes on mixed flow pump impeller. *Turbomach. Soc. Jpn.* **2002**, *30*, 70–75. (In Japanese)
8. Hitachi Plant Technologies. *PBO, Internal Technical Report CWP No. MR-110519-15-114-001*; 2012; Unpublished.
9. Li, X.-H.; Zhang, S.-J.; Zhu, B.-L.; Hu, Q.-B. The study of the k-ε turbulence model for numerical simulation of centrifugal pump. In Proceedings of the 7th International Conference on Computer-Aided Industrial Design and Conceptual Design, Hangzhou, China, 17–19 November 2006; pp. 1–5.
10. American National Standard. *Rotodynamic Vertical Pumps of Radial, Mixed, and Axial Flow Types*; ANSI/HI 2.3-2013; Hydraulic Institute: Parsippany, NJ, USA, 2013.
11. Alpan, K.; Peng, W.W. Suction reverse flow in an axial-flow pump. *J. Fluids Eng. ASME Trans.* **1991**, *113*, 90–97. [CrossRef]
12. Ingersoll-Rand Company. *Test Standards for Modelling Inlets to Pumps*; Ingersoll-Rand Company: Phillipsburg, NJ, USA, 1991.
13. U.S. Army Corps of Engineers. *Mechanical and Electrical Design of Pumping Stations EM 1110-2-3105*; U.S. Army Corps of Engineers: Washington, DC, USA, 1999.
14. Arocena, V.M.; Abuan, B.E.; Reyes, J.G.T.; Rodgers, P.L.; Danao, L.A.M. Reduction of Entrained Vortices in Submersible Pump Suction Lines Using Numerical Simulations. *Energies* **2020**, *13*, 6136. [CrossRef]
15. Hecker, G.E. Model-prototype comparison of free surface vortices. *J. Hydraul. Div.* **1981**, *107*, 1243–1259. [CrossRef]
16. Qian, Z.; Wu, P.; Guo, Z.; Huai, W.-X. Numerical simulation of air entrainment and suppression in pump. *Sci. China Technol. Sci.* **2016**, *59*, 1847–1855. [CrossRef]
17. Ahn, S.-H.; Xiao, Y.; Wang, Z.; Zhou, X.; Luo, Y. Numerical prediction on the effect of free surface vortex on intake flow characteristics for tidal power stations. *Renew. Energy* **2017**, *101*, 617–628. [CrossRef]
18. Menter, F. Review of the shear-stress transport turbulence model experience from an industrial perspective. *Int. J. Comput. Fluid Dyn.* **2009**, *23*, 305–316. [CrossRef]
19. Knauss, J. Swirling flow problems at intakes. In *IAHR Hydraulic Structures Design Manual*; A.A. Balkema: Rotterdam, The Netherlands, 1987; Volume 1.
20. ANSYS, Inc. *ANSYS Fluent Theory Guide*; ANSYS, Inc.: Canonsburg, PA, USA, 2018.